Understanding the Inhibiting Effect of BTC on CuBTC Growth through Experiment and Modeling

Schäfer, Philipp; Kapteijn, Freek; Van Der Veen, Monique A.; Domke, Katrin F.

DOI
10.1021/acs.cgd.7b00938

Publication date
2017

Document Version
Final published version

Published in
Crystal Growth & Design

Citation (APA)
Schäfer, P., Kapteijn, F., Van Der Veen, M. A., & Domke, K. F. (2017). Understanding the Inhibiting Effect of BTC on CuBTC Growth through Experiment and Modeling. *Crystal Growth & Design*, *17*(11), 5603-5607. https://doi.org/10.1021/acs.cgd.7b00938

CRYSTAL GROWTH & DESIGN

Communication

pubs.acs.org/crystal

Understanding the Inhibiting Effect of BTC on CuBTC Growth through Experiment and Modeling

Philipp Schäfer,[†] Freek Kapteijn,[‡] Monique A. van der Veen,*[,‡] and Katrin F. Domke*[,†]

[†]Max Planck Institute for Polymer Research, Molecular Spectroscopy Department, Ackermannweg 10, D55128 Mainz, Germany

[‡]Delft University of Technology, Faculty of Applied Sciences, Chemical Engineering Department, Section of Catalysis Engineering, Van der Maasweg 9, NL 2629 HZ Delft, The Netherlands

Supporting Information

ABSTRACT: The room temperature growth kinetics of the commonly studied metal−organic framework CuBTC (HKUST-1) is investigated with UV/vis absorption spectroscopy. Contrary to chemical intuition, increased concentrations of the BTC ligand slows down the formation of CuBTC. Based on the time-resolved experimental data, a kinetic model is proposed for CuBTC growth. This model is based on a chemical reaction equation sequence for the production of CuBTC including an overcoordinated, slowly reacting Cu-BTCx species. This growth model excellently captures the temporal CuBTC development over the entire range of concentration conditions.

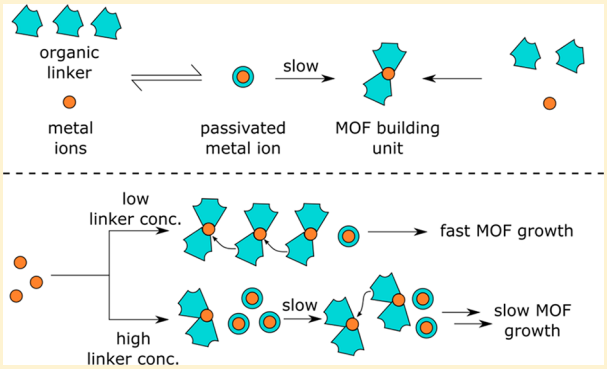

Metal−organic frameworks (MOFs), an intriguing class of hybrid crystalline materials consisting of metal cations or oxo-clusters coordinated with multifunctional organic linkers, are drawing increasing attention from the scientifc community because the tunable nano- to mesoporous crystalline structure in combination with diverse functionality holds great promise for interesting applications in gas sensing,[1,2] storage and sieving,[3,4] catalysis,[5−7] and drug delivery.[8] While the crystallographic properties of MOFs, such as their morphology and underlying crystal structure, as well as the coordination geometry within the crystal are routinely investigated,[9,10] the rich but hard to assess coordination chemistry during solvothermal MOF synthesis is rarely studied. To optimize large-scale production for high yields and fast reaction turnover and to facilitate rational synthetic design of material ensemble properties, e.g., crystallinity and size dispersion, however, insight into the complete reaction sequence and kinetics of the elementary reactions during solvothermal MOF synthesis is urgently required.

One of the best-known MOFs, CuBTC (HKUST-1; BTC: 1,3,5-benzenetricarboxylic acid), serves as one of the workhorses for unraveling mechanisms underlying MOF formation[11−13] and MOF−adsorbate interactions.[14−16] Commonly, CuBTC is synthesized solvothermally at elevated temperature and pressure[17−19] or at room temperature[20] in organic solvent/water solutions with varying water contents up to 50% from a Cu salt (e.g., $Cu(NO_3)_2$) and BTC in concentrations near saturation of 100 to 200 mM.

While nucleation and growth of CuBTC have been studied in situ with X-ray diffraction[21] or light scattering,[22] little is known about the coordination chemistry during the synthesis. For example, the Cu paddlewheel MOF subunit, a dinuclear Cu center bridged by four BTC ligands that interconnects into a larger network, is a commonly observed coordination motif in crystalline structures of Cu carboxylate MOFs.[23,24] However, the detailed role of the paddlewheel formation and possible intermediate species and side-reactions for the kinetics of MOF nucleation and growth has remained unclear. Here, we set out to understand the coordination chemistry during homogeneous CuBTC nucleation and growth and to unravel how the interplay of Cu^{2+} and BTC influences the kinetics of CuBTC formation.

While previous kinetic investigations have mainly focused on the effect of the synthesis temperature at fixed concentrations,[25] here we investigate the effect of reactant concentrations on the kinetics of room-temperature CuBTC growth and on the chemical composition of the solution. We have developed a kinetic model based on a chemical reaction sequence that we numerically evaluate against the temporal experimental growth data to capture the role of the reactant concentrations during synthesis.

Figure 1a shows time-dependent UV/vis absorbance spectra measured for a 1 mM Cu^{2+} and 18 mM BTC ethanolic solution. The first spectrum (light gray, measured 20 s after mixing the solution) shows a single absorbance with a maximum of ca. 0.025 AU (absorbance unit) at 800 nm that closely matches the signature of a pure 1 mM $Cu(NO_3)_2 \times 2.5$ H_2O solution (SI, Figure S2). This species is most likely a

Received: July 5, 2017
Revised: September 28, 2017
Published: October 12, 2017

DOI: 10.1021/acs.cgd.7b00938
Cryst. Growth Des. 2017, 17, 5603−5607

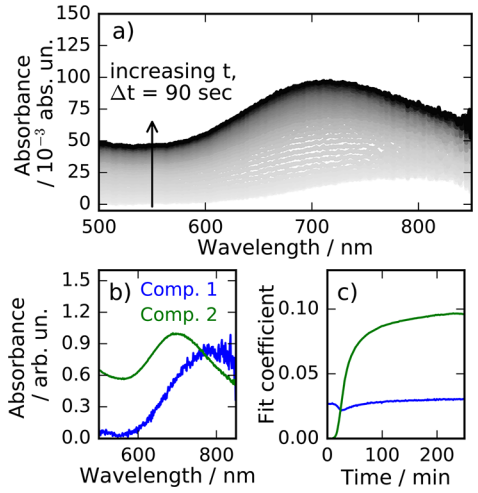

Figure 1. Overview over a single UV/vis kinetic measurement. (a) UV/vis absorption spectra at 90 s intervals in 1 mM Cu^{2+}/18 mM BTC ethanolic solution. (b) Spectra taken as the two component spectra for the non-negative least-squares fit as described in eq (12) in the SI. (c) Evolution of the fit coefficients for the two components over the time of the experiment.

Cu^{2+}-hydrate-nitrate complex, a Jahn−Teller distorted octahedral complex with ethanol/water in the equatorial positions and the labile nitrate in the axial positions.[26] The absorption stems from a d−d transition in Cu^{2+}. With time, the spectral intensity increases and a second aborbance of ca. 0.1 AU appears at ca. 710 nm after around 100 min that matches the d−d transition absorption of CuBTC reported in literature.[27,28]

To investigate the synthesis kinetics of CuBTC, the spectral contributions of the precursor and of CuBTC (Figure 1) are deconvoluted by non-negative least-squares (NNLS) fitting with two components (Figure 1b). Component 1 is ethanolic $Cu(NO_3)_2 \times 2.5\ H_2O$ and component 2 is taken from a separate NNLS fit with a free floating spectral component (details in SI, section 4) identified as CuBTC. According to Lambert−Beer's law, the measured absorption is directly proportional to the concentration of a chemical species. The measured spectra are taken as a superposition of the two components weighted by a fit coefficient taken from the NNLS fit, which is proportional to the concentration of the species in the solution.

Figure 1 c shows the time traces of the extracted NNLS fit coefficients. The contribution of component spectrum 1 is maximal at the beginning of the experiment and starts decreasing after ≈10 min. After 20 min, a minimum is reached after which the contribution increases again. The coefficient for component 2 (green) is 0 in the beginning. After an induction period of 10 min, coefficient 2 starts increasing, reaching its maximum slope after around 25 min until it starts leveling off, approaching saturation at around 0.1 AU after 100 min (details see SI, section 4.1).

Figure 2 shows the fit coefficients for component 2 (CuBTC) for different BTC (Figure 2a) and (Figure 2b) concentrations, respectively, as a function of time. The BTC:Cu ratios range from 9:1 to 93:1. The spectra used for the NNLS fit are those shown in Figure 1 b. All traces show similar behavior: after an induction period, the coefficient increases before leveling off after different times. Interestingly, the induction time gradually increases with BTC concentration from being hardly resolvable for 9 mM BTC to about 350 min

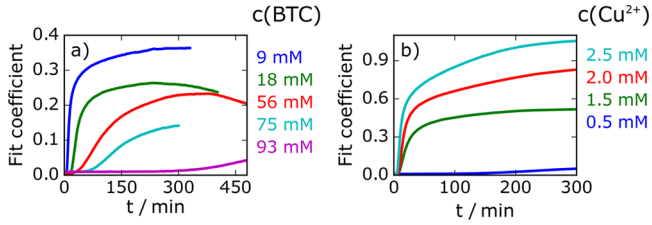

Figure 2. (a) Fit coefficient vs time at different BTC concentrations as noted in the legend and constant 1 mM Cu^{2+} concentration. (b) Fit coefficient vs time at different Cu^{2+} concentrations as noted in the legend and constant 38 mM BTC concentration.

for 93 mM BTC. The growth rate after the induction period decreases with increasing BTC concentration where for the lowest (highest) BTC concentration of 9 mM (93 mM), the maximum slope is around 2×10^{-2} min^{-1} (2×10^{-4} min^{-1}). Contrary to chemical intuition, increasing BTC concentration hinders the formation of CuBTC by increasing the induction period and slowing down the growth rate. The drop in the fit coefficient toward later times in some traces results from CuBTC crystals precipitating in the cuvette, i.e., moving out of the probed sample volume.

For increasing Cu^{2+} and constant 38 mM BTC concentrations, the induction period shortens while the growth rate increases (Figure 2b). For the lowest (highest) Cu^{2+} concentration of 0.5 mM (2.5 mM), the maximum slope is around 3×10^{-4} min^{-1} (4×10^{-2} min^{-1}). The total maximum CuBTC contribution increases with Cu^{2+} concentration, indicating that Cu^{2+} concentration is the yield-limiting factor in this CuBTC synthesis.

In the following, a phenomenological chemical reaction model is proposed that accounts for the "incubation" period, the increase in rate, the leveling off of the traces, and the inhibiting effect of BTC on the reaction. First, the incubation period and increase in growth rate toward the middle of the growth can be explained with a nucleation−growth model as already proposed for several crystal-growth mechanisms, e.g., by Lutsko et al. for zeolites.[29] In essence, nucleation is usually thermodynamically "uphill" and thus hindered while growth onto an already existing nucleus or crystal surface is energetically favorable and thus faster because of cooperative effects. We formulate two equations describing these distinct formation stages where the initial solvated Cu^{2+} species is discussed as Cu to simplify the phenomenological reaction equations regarding charge balance. A detailed assignment of charges (especially for the BTC molecule) would require additional information about the protonation state of the linker during the reaction that is unavailable through our experiments. The nucleation reaction of our system can be described as

$$2Cu + 4BTC \xrightarrow{k_1} Cu_2BTC_4 \quad (1)$$

where Cu_2BTC_4 is the dinuclear Cu-paddlewheel, i.e., the fundamental building unit of CuBTC-MOF. While it is debatable whether a single Cu-paddlewheel already serves as a reactive nucleus, this description suffices in our phenomenological model. For crystal growth catalyzed by existing CuBTC-MOF surface, we formulate

$$[Cu_2BTC_4] + 2Cu + 3BTC \xrightarrow{k_1} [Cu_2BTC_4]\cdots Cu_2BTC_3 \quad (2)$$

DOI: 10.1021/acs.cgd.7b00938
Cryst. Growth Des. 2017, 17, 5603−5607

where $[Cu_2BTC_4]$ denotes a surface site on an existing CuBTC crystal that serves as an anchor point for the next building unit. We assume that only three free BTC molecules are needed to attach a new building unit. The last BTC molecule to complete the paddlewheel could be one that is part of an already existing CuBTC crystal and is used as an anchor for the new paddlewheel unit. The attachment of a complete dinuclear paddlewheel unit (Cu_2BTC_3) is consistent with *in situ* AFM studies of John et al., who observed that CuBTC grows stepwise with an observed step height matching the height of a single paddlewheel unit.[30] Equation 2 does not yield the expected stochiometry of HKUST-1, namely, Cu_3BTC_2. As more building-units add onto the existing crystal, some will attach to corner sites, where two BTC molecules (and later possibly even three) are already present, and fewer BTC molecules from the solution have to be added. Over time the whole crystal will then approach the 3:2 stochiometry. Information about the order and extent of these different attachments is unfortunately not available from our experiments, which is why we discuss the more elementary and "earlier" reactions.

Furthermore, the model has to explain the inhibiting behavior of the ligand, i.e., BTC must be part of a competing chemical reaction step that leads to a formation of a species that does not react to CuBTC or only does so slowly. Otherwise, an increase in the linker concentration would, according to eqs 2 and 1, lead to an increase in the growth rate. Formation of such an "inactive" species must be favored over the formation of the desired product Cu_2BTC_4 at high concentrations of BTC. This requirement is fulfilled when the stochiometric BTC/Cu ratio is larger in the reaction that forms the slowly reacting species than in that of the MOF itself, i.e., when an increase in BTC concentration leads to an overall decrease in the production rate of Cu_2BTC_4. Hence, a reaction is proposed that describes the reversible formation of a species CuBTCx that is overcoordinated in BTC and can only slowly react to the desired product:

$$\mathrm{Cu} + x\mathrm{BTC} \underset{K_{3r}}{\overset{K_3}{\leftrightarrow}} \mathrm{CuBTC}_x \tag{3}$$

To investigate structure and coordination number x of CuBTCx, the UV/vis absorbance spectra of solutions with different BTC concentrations are analyzed at a constant 1 mM Cu concentration within 20 s after mixing the solutions (Figure 3 a). While for low BTC concentrations of 9 mM and 18 mM, the spectra resemble the one of ethanolic $Cu(NO_3)_2 \times 2.5H_2O$, solutions with higher BTC concentrations show a gradual increase in the total absorbance intensity and a blue shift of the absorbance maximum from 800 nm for 9 mM BTC to 740 nm for 138 mM BTC. The blue shift cannot be due to an immediate formation of CuBTC as the CuBTC growth is significantly slowed down at high BTC concentrations (Figure 2), but indicates the presence of a third spectroscopically identifiable component with an absorbance maximum at 740 nm between the maxima of components 1 and 2. This third component cannot be fitted because its spectrum can mathematically be described as a linear combination of components 1 and 2. However, assuming a reaction as described in eq 3, we can infer that given concentrations of BTC and Cu lead to a defined chemical equilibrium before the actual growth of CuBTC starts to have a significant effect on the concentrations in the solution (mathematical derivation see SI, section 5). We expect the integrated UV/vis absorbance over the investigated spectral range to follow formula 4

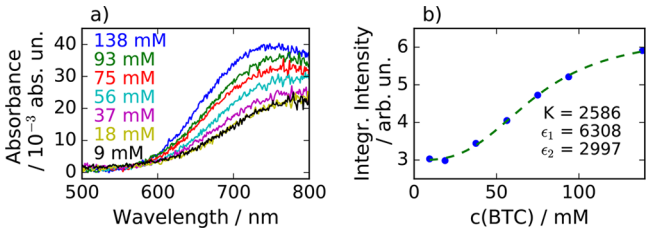

Figure 3. (a) UV/vis spectra taken of growth solutions at different BTC concentrations immediately after mixing the components. (b) Integrated intensity of the UV/vis spectra in (a) in the range from 500 to 800 nm vs the concentration of BTC in the solution. The green line shows a fit of the data to eq 4. The inset text shows the resulting parameters for K, ε_1, and ε_2.

$$I_{\mathrm{tot}} = \frac{c_0(\mathrm{Cu})}{1 + Kc_0(\mathrm{BTC})^x} \cdot (\varepsilon_1 + \varepsilon_2 \cdot K \cdot c_0(\mathrm{BTC})^x) \tag{4}$$

with c_0(Cu) and c_0(BTC) the starting concentrations of Cu-ions and of BTC, respectively, K the equilibrium constant for reaction 3, x the coordination number and ε_1 and ε_2 the integrated absorbance coefficients for the two fitted components over the investigated wavelength range. Figure 3b shows the integrated total intensities of the spectra in (a) and the fit of the experimental data to eq 4 assuming a coordination number of $x = 3$ (green line). The data can also be fitted reasonably well with a coordination number of $x = 2$ (SI, Figure S4). If one BTC molecule occupies two coordination sites around the Cu center through one carboxyl moiety, both coordination numbers lead to commonly observed structures of Cu^{II} complexes, with $x = 2$ a square planar configuration and $x = 3$ a Jahn−Teller distorted octahedral complex.[31] A dinuclear Cu complex with 6 acetate ligands and a structure similar to the CuBTC paddlewheel has been observed previously and fits the 1/3 Cu^{2+}/BTC ratio as well.[32]

Based on the discussion above, we propose the following reaction for our model:

$$\mathrm{Cu} + 3\mathrm{BTC} \underset{K_{3r}}{\overset{K_3}{\leftrightarrow}} \mathrm{CuBTC}_3 \tag{5}$$

in addition to a reaction sequence that allows this newly proposed $CuBTC_3$ species to react to the desired MOF product at an existing crystal surface, analogous to the crystal growth reaction in eq2

$$2\mathrm{CuBTC}_3 + [\mathrm{Cu}_2\mathrm{BTC}_4] \xrightarrow{k_4} [\mathrm{Cu}_2\mathrm{BTC}_4]\cdots \mathrm{Cu}_2\mathrm{BTC}_3 + 3\mathrm{BTC} \tag{6}$$

The simulated temporal concentration profiles based on the proposed set of reactions in eqs 1, 2, 5, and 6 under specific experimental conditions (simulation details, see SI) are given in Figure 4.

The concentration of CuBTC over an arbitrary time scale for different BTC and constant 1 mM Cu^{2+} concentrations is 0 at the beginning of the simulation for all traces. After an induction period whose length increases with BTC concentration, growth of CuBTC starts; for 10 mM BTC, the induction period lasts around 2000 time units while for the highest simulated BTC concentration of 150 mM, it lasts around 15000 time units. The maximum rate, i.e., the maximum slope of the traces, decreases

DOI: 10.1021/acs.cgd.7b00938
Cryst. Growth Des. 2017, 17, 5603−5607

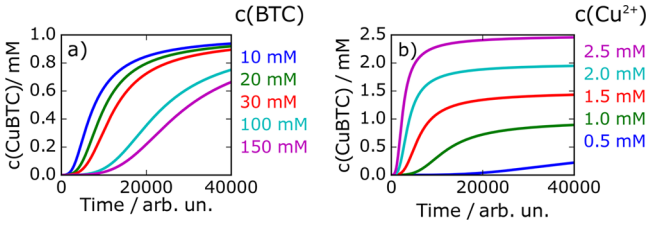

Figure 4. Results of the numerical evaluation of the reaction model. (a) CuBTC concentration vs time for different BTC and starting 1 mM Cu^{2+} concentrations. (b) CuBTC concentration vs time/number of simulation steps at different starting $Cu^{2+}$and constant 30 mM BTC concentrations.

with higher BTC concentrations from 1×10^{-7} mM/time for 10 mM BTC to 3×10^{-8} mM/time for 150 mM BTC. Toward the end, the changes in CuBTC concentration level off and approach a maximum limit. For different Cu^{2+} concentrations and constant 30 mM BTC (Figure 4b), the induction period shortens with increasing Cu^{2+} concentration (20000 (1000) time units at 0.5 (2.5) mM) and the maximum rate of the traces increases by nearly 2 orders of magnitude from 1×10^{-8} mM/time. at 0.5 mM Cu^{2+} to 8×10^{-7} mM/time at 2.5 mM Cu^{2+}. The simulated traces qualitatively match the measured data and reproduce all important features such as the induction period of the growth, the leveling off due to a decrease in active Cu^{2+} species toward the end, the increase in overall rate at higher Cu^{2+} concentrations, and the inhibiting effect of higher BTC concentrations on the overall growth process. Additionally, a characterization of CuBTC samples synthesized under different concentration conditions (SI Figure S5) shows a slight crystal-size increase with higher BTC concentrations consistent with our proposal of the formation of a non-nucleating and slowly reacting $CuBTC_x$ species.

It is known from *in situ* atomic force microscopy[30] and quartz crystal microbalance[26] measurements that CuBTC generally grows layer by layer, i.e., complete paddlewheel structures attach to an already existing MOF surface. While in reality, reactions 2 and 6 can be expected to go through a preformed intermittent paddlewheel state, we want to emphasize that our model minimizes the number of chemical equations to the absolutely necessary ones to capture the experimental results.

It should be noted that we cannot verify our kinetic model in experiments with a BTC:Cu ratio closer to the conditions used in literature (1:2[22] compared to our 9 to 93:1) to produce CuBTC. At lower ratios, the nucleation and growth proceed too quickly to be measured with our time resolution of 90 s/spectrum. We, however, do not expect the fundamental coordination chemistry of the system to change drastically at different linker/metal ion ratios. As our model is able to explain the experimental data of all investigated metal/linker ratios, we do not expect the presence of any additional UV/vis detectable coordination compounds. Therefore, higher Cu/BTC ratios should only influence the reaction kinetics as predicted by our model.

In summary, the progress of room-temperature CuBTC growth in solution is analyzed with UV/vis spectroscopy. The CuBTC contribution is separated from the precursor contribution with the help of NNLS fitting to obtain kinetic information about the MOF growth process. In this first concentration-dependence study of CuBTC growth, we observe that while an increase in the Cu^{2+} concentration leads to an increase in the reaction rate, a high BTC concentration slows down the growth because of the formation of a BTC-overcoordinated $CuBTC_x$ species that only slowly reacts to CuBTC MOF. Based on our observations, a chemical reaction sequence is proposed to describe CuBTC nucleation and growth, including the inhibiting effect of BTC. The derived kinetic model exhibits an excellent qualitative correlation to the experimental data. Our results underline the importance of a detailed insight into reaction kinetics for, e.g., the engineering of large-scale production facilities that aim for a fast production turnover. Our findings suggest an optimized BTC concentration if fast production of CuBTC is desired. Future studies on the fundamental coordination chemistry during synthesis of other MOFs should be conducted to explore a possible universality of our model.

■ ASSOCIATED CONTENT

Supporting Information

The Supporting Information is available free of charge on the ACS Publications website at DOI: 10.1021/acs.cgd.7b00938.

Experimental details, details on the fitting and the numerical modeling, mathematical background, characterization of synthesized material (PDF)

■ AUTHOR INFORMATION

Corresponding Authors

*E-mail: M.A.vanderVeen@tudelft.nl.
*E-mail: domke@mpip-mainz.mpg.de.

ORCID

Freek Kapteijn: 0000-0003-0575-7953
Monique A. van der Veen: 0000-0002-0316-4639
Katrin F. Domke: 0000-0002-4562-6088

Notes

The authors declare no competing financial interest.

■ ACKNOWLEDGMENTS

K.F.D. acknowledges generous support through the Emmy Noether program of the Deutsche Forschungsgemeinschaft (#DO1691/1-1) and through the European Commission Marie Curie Actions (ITN-FINON #607842). P.S. is grateful for a PhD fellowship of the Max Planck Graduate Center Mainz and the Studienstiftung des dt. Volkes. The authors thank Marialore Sulpizi for fruitful discussions.

■ REFERENCES

(1) Kreno, L. E.; Hupp, J. T.; Van Duyne, R. P. Metal-organic framework thin film for enhanced localized surface plasmon resonance gas sensing. *Anal. Chem.* **2010**, *82*, 8042−6.

(2) Liu, J.; Sun, F. X.; Zhang, F.; Wang, Z.; Zhang, R.; Wang, C.; Qiu, S. L. In situ growth of continuous thin metal-organic framework film for capacitive humidity sensing. *J. Mater. Chem.* **2011**, *21*, 3775−3778.

(3) Asadi, T.; Ehsani, M. R.; Ribeiro, A. M.; Loureiro, J. M.; Rodrigues, A. E. CO 2 /CH 4 Separation by Adsorption using Nanoporous Metal organic Framework Copper-Benzene-1,3,5-tricarboxylate Tablet. *Chem. Eng. Technol.* **2013**, *36*, 1231−1239.

(4) Teufel, J.; Oh, H.; Hirscher, M.; Wahiduzzaman, M.; Zhechkov, L.; Kuc, A.; Heine, T.; Denysenko, D.; Volkmer, D. MFU-4 − A MetalOrganic Framework for Highly Effective H2/D2 Separation. *Adv. Mater.* **2013**, *25*, 635−639.

(5) Yoon, M.; Srirambalaji, R.; Kim, K. Metalorganic frameworks—prospective industrial applications. *Chem. Rev.* **2012**, *112*, 1196−1231.

(6) Wang, J.-L.; Wang, C.; Lin, W. MetalOrganic Frameworks for Light Harvesting and Photocatalysis. *ACS Catal.* **2012**, *2*, 2630−2640.

DOI: 10.1021/acs.cgd.7b00938
Cryst. Growth Des. 2017, 17, 5603−5607

(7) Kesanli, B.; Lin, W. Chiral porous coordination networks: rational design and applications in enantioselective processes. *Coord. Chem. Rev.* **2003**, *246*, 305−326.
(8) Horcajada, P.; Serre, C.; Vallet-Regí, M.; Sebban, M.; Taulelle, F.; Férey, G. MetalOrganic Frameworks as Efficient Materials for Drug Delivery. *Angew. Chem., Int. Ed.* **2006**, *45*, 5974−5978.
(9) Dybtsev, D. N.; Chun, H.; Kim, K. Rigid and flexible: A highly porous metalorganic framework with unusual guest-dependent dynamic behavior. *Angew. Chem., Int. Ed.* **2004**, *43*, 5033−5036.
(10) Kramer, M.; Schwarz, U.; Kaskel, S. Synthesis and properties of the metal-organic framework Mo3(BTC)2 (TUDMOF-1). *J. Mater. Chem.* **2006**, *16*, 2245−2248.
(11) Shekhah, O.; Wang, H.; Zacher, D.; Fischer, R. A.; Wöll, C. Growth mechanism of metal-organic frameworks: insights into the nucleation by employing a step-by-step route. *Angew. Chem., Int. Ed.* **2009**, *48*, 5038−41.
(12) Stavila, V.; Volponi, J.; Katzenmeyer, A. M.; Dixon, M. C.; Allendorf, M. D. Kinetics and mechanism of metal−organic framework thin film growth: systematic investigation of HKUST-1 deposition on QCM electrodes. *Chemical Science* **2012**, *3*, 1531−1540.
(13) Shöâeé, M.; Anderson, M. W.; Attfield, M. P. Crystal Growth of the Nanoporous Metal-Organic Framework HKUST-1 Revealed by In Situ Atomic Force Microscopy. *Angew. Chem., Int. Ed.* **2008**, *47*, 8525−8528.
(14) Skoulidas, A. I. Molecular Dynamics Simulations of Gas Diffusion in Metal−Organic Frameworks: Argon in CuBTC. *J. Am. Chem. Soc.* **2004**, *126*, 1356−1357.
(15) YazaydIn, A. O.; Benin, A. I.; Faheem, S. A.; Jakubczak, P.; Low, J. J.; Willis, R. R.; Snurr, R. Q. Enhanced CO2 Adsorption in Metal-Organic Frameworks via Occupation of Open-Metal Sites by Coordinated Water Molecules. *Chem. Mater.* **2009**, *21*, 1425−1430.
(16) García-Pérez, E.; Gascón, J.; Morales-Flórez, V.; Castillo, J. M.; Kapteijn, F.; Calero, S. Identification of Adsorption Sites in Cu-BTC by Experimentation and Molecular Simulation. *Langmuir* **2009**, *25*, 1725−1731.
(17) Chui, S. S. Y.; Lo, S. M. F.; Charmant, J. P. H.; Orpen, a. G.; Williams, I. D. A Chemically Functionalizable Nanoporous Material [Cu3(TMA)2(H2O)3]n. *Science* **1999**, *283*, 1148−1150.
(18) Kim, K.-J.; Li, Y. J.; Kreider, P. B.; Chang, C.-H.; Wannenmacher, N. High-rate synthesis of Cu−BTC metal−organic frameworks. *Chem. Commun.* **2013**, *49*, 11518.
(19) Kim, J.; Cho, H.-Y.; Ahn, W.-S. Synthesis and Adsorption/Catalytic Properties of the Metal Organic Framework CuBTC. *Catal. Surv. Asia* **2012**, *16*, 106−119.
(20) Zhuang, J.-L.; Ceglarek, D.; Pethuraj, S.; Terfort, A. Rapid Room-Temperature Synthesis of Metal-Organic Framework HKUST-1 Crystals in Bulk and as Oriented and Patterned Thin Films. *Adv. Funct. Mater.* **2011**, *21*, 1442−1447.
(21) Millange, F.; Medina, M. I.; Guillou, N.; Férey, G.; Golden, K. M.; Walton, R. I. Time-Resolved In Situ Diffraction Study of the Solvothermal Crystallization of Some Prototypical Metal-Organic Frameworks. *Angew. Chem., Int. Ed.* **2010**, *49*, 763−766.
(22) Zacher, D.; Liu, J.; Huber, K.; Fischer, R. A. Nanocrystals of [Cu3(btc)2] (HKUST-1): a combined time-resolved light scattering and scanning electron microscopy study. *Chem. Commun.* **2009**, 1031−1033.
(23) Jenniefer, S. J.; Muthiah, P. T. Synthesis, characterization and X-ray structural studies of four copper (II) complexes containing dinuclear paddle wheel structures. *Chem. Cent. J.* **2013**, *7*, 35.
(24) Kyuzou, M.; Mori, W.; Tanaka, J. Electronic structure and spectra of cupric acetate mono-hydrate revisited. *Inorg. Chim. Acta* **2010**, *363*, 930−934.
(25) Millange, F.; El Osta, R.; Medina, M. E.; Walton, R. I. A time-resolved diffraction study of a window of stability in the synthesis of a copper carboxylate metal−organic framework. *CrystEngComm* **2011**, *13*, 103−108.
(26) Shekhah, O.; Wang, H.; Zacher, D.; Fischer, R. A.; Wöll, C. Growth Mechanism of Metal-Organic Frameworks: Insights into the Nucleation by Employing a Step-by-Step Route. *Angew. Chem., Int. Ed.* **2009**, *48*, 5038−5041.
(27) Borfecchia, E.; Maurelli, S.; Gianolio, D.; Groppo, E.; Chiesa, M.; Bonino, F.; Lamberti, C. Insights into Adsorption of NH3 on HKUST-1 Metal−Organic Framework: A Multitechnique Approach. *J. Phys. Chem. C* **2012**, *116*, 19839−19850.
(28) Li, Z.-Q.; Wang, A.; Guo, C.-Y.; Tai, Y.-F.; Qiu, L.-G. Insights into Adsorption of NH3 on HKUST-1 Metal−Organic Framework: A Multitechnique Approach. *Dalton Transactions* **2013**, *42*, 13948.
(29) Lutsko, J. F.; Basios, V.; Nicolis, G.; Caremans, T. P.; Aerts, A.; Martens, J. A.; Kirschhock, C. E. A.; van Erp, T. S. Kinetics of intermediate-mediated self-assembly in nanosized materials: A generic model. *J. Chem. Phys.* **2010**, *132*, 164701.
(30) John, N. S.; Scherb, C.; Shöâeè, M.; Anderson, M. W.; Attfield, M. P.; Bein, T. Single layer growth of sub-micron metal-organic framework crystals observed by in situ atomic force microscopy. *Chem. Commun.* **2009**, *2*, 6294−6296.
(31) Gaâzo, J.; Bersuker, I.; Garaj, J.; Kabešová, M.; Kohout, J.; Langfelderová, H.; Melník, M.; Serator, M.; Valach, F. Plasticity of the coordination sphere of copper(II) complexes, its manifestation and causes. *Coord. Chem. Rev.* **1976**, *19*, 253−297.
(32) Sharrock, P.; Melník, M. Copper(II) acetates: from dimer to monomer. *Can. J. Chem.* **1985**, *63*, 52−56.

DOI: 10.1021/acs.cgd.7b00938
Cryst. Growth Des. 2017, 17, 5603−5607